28. Steady-State Thermal Convection Currents in the Earth's Asthenosphere Inferred from Gravity and Heat Flow Data.

By Yukio HAGIWARA,

Earthquake Research Institute, University of Tokyo.

Abstract

Steady-state convection currents of an incompressible Newtonian fluid of very high viscosity in a non-rotating spherical-shell model of the earth's asthenosphere are solved, using the spherical surface harmonic representations of the temperature and fluid velocity fields. The gravity anomaly related to the convection-induced density change is also expressed in a spherical surface harmonic series. The gravity anomaly thus calculated is compared with the gravity data obtained from satellite orbit analyses so as to maximize the mutual correlation coefficient between the two gravity anomalies.

As a result, the gravity anomaly calculated with a uniform viscosity of 3.5×10^{19} N. s. m^{-2} for an asthenosphere model having a thickness of 300 km or 1.5×10^{20} N. s. m^{-2} for one having a thickness of 400 km is found to be consistent with the satellite-derived gravity data. It is demonstrated that both gravity anomalies match each other up to some detailed features, for example, the positive anomaly on the Mid-Atlantic Ridge, the negative one widely located in the Mid-Asian continent and the Indian Ocean, etc.

1. Introduction

The theory of convection currents with its application to two-dimensional fluid mantle models has been investigated by many authors for the purpose of explaining the geophysical facts observed along mid-ocean ridges and deep-sea trenches. For example, McKENZIE et al. (1974) have shown that, based on results of two-dimensional numerical experiments, the gravity-heat flow relationship obtained in the Mid-Atlantic regions is explainable by considering the contribution from the deformed surface.

Recently, Kono *et al.* (1979) have investigated the time-dependent be-
haviors of two-dimensional fluid models with variable viscosity in rela-
tion to the heat flow profile observed near the East-Pacific Rise.

The two-dimensional approach, however, is essentially inappropriate
for understanding the global geophysical phenomena in the spherical
earth. The model to be adopted for investigating convection in the earth's
asthenosphere is a spherical shell, because it can be well approximated
to the shape of the real asthenosphere, except for the equatorial bulge
and the boundary undulation. In this case, the convecting fluid behavior
can be described in mathematical expressions of fluid dynamical equations
using spherical surface harmonic functions.

Similarly to the ideas of Chandrasekhar (1961) and Runcorn (1964),
this paper treats steady-state convection currents of an incompressible
Newtonian fluid of very high viscosity in a non-rotating spherical shell.
Despite the simplifications, the mathematical treatment is still so com-
plicated that numerical computations using finite difference methods
sometimes result in unstable solutions. In order to overcome such a
difficulty, this paper treats the derivations of analytical solutions in some
justifiable mathematical approximations which would not affect the
qualitative features of the anticipated convection currents. The simplified
formulation is considered to retain the significant global features of
mantle convection without loss of essential generality.

The first attempt in this paper is to establish a one-to-one mathe-
matical relationship between outside gravity field and terrestrial heat
flow. This relationship is based on an idea similar to the two-dimensional
analytical method previously proposed by the author (Hagiwara, 1980).
Secondly, a gravity anomaly calculated from the global heat flow data
(Chapman and Pollack, 1975) is compared with that determined by the
satellite orbit analyses (Gaposchkin, 1973). The coincidence between the
observed gravity anomaly and the calculated one may confirm the pre-
supposed theoretical simplifications and physical properties of the con-
vection model, and further may provide us with the knowledge of what
properties act effectively on convection patterns under given boundary
conditions. In this sense, our discussion will concentrate on how to
obtain the convection model most suitable to the observed gravity field.

2. Formulation of Convection

The thermal convection of incompressible viscous fluid is described in
the Stokes and Boussinesq approximations of equations of fluid motion,

continuity, thermal conduction, and state. The non-linear terms in these equations are eliminated by the perturbation method, assuming that all second and higher order terms in the perturbation variables (called "anomaly" hereafter in this paper) are negligibly small as compared with the static solution. Then, the linear steady-state perturbation equation are expressed as

$$\mu \nabla^2 \boldsymbol{v} = \operatorname{grad} p + \rho \boldsymbol{g} , \tag{1}$$

$$k \nabla^2 T = \boldsymbol{v} \operatorname{grad} \bar{T} , \tag{2}$$

$$\rho = -\alpha \rho_0 T , \tag{3}$$

with the equation of continuity

$$\operatorname{div} \boldsymbol{v} = 0 . \tag{4}$$

In the above notations, μ is the coefficient of viscosity, $\boldsymbol{v}$ the fluid velocity vector, p the pressure anomaly, ρ the density anomaly, ρ_0 the mean density, $\boldsymbol{g}$ the gravity vector acting in the spherocentric direction, k the thermal diffusivity, T the temperature anomaly, $\bar{T}$ the static temperature and α the coefficient of thermal expansion.

For applying these equations to the thermal convection model of the earth's asthenosphere, the radial variations in gravity and static temperature are first assumed as follows:

$$g_r = g_0 \frac{r}{b} , \tag{5}$$

$$\bar{T} = T_0 + \beta(b^2 - r^2) , \tag{6}$$

where b, g_0 and T_0 are the outer radius of the asthenosphere, the mean gravity and the mean temperature at $r = b$, respectively, and β is taken to be constant. The gravity field (5) is realized if the convecting layer has a uniform density, but is somewhat different from the real internal gravity field (*e.g.*, HADDON and BULLEN, 1969). The radial temperature distribution in the real mantle is also different from (6) (*e. g.*, RIKITAKE, 1952). However, since the problem is treated in a thin spherical shell, such simplifications can not essentially affect the qualitative features of the postulated convection flows.

The velocity field is assumed to be expressed by a scalar function W and the radial vector $\boldsymbol{r}$ as follows:

$$\boldsymbol{v} = \operatorname{curl} (\operatorname{grad} W \times \boldsymbol{r}) ,$$

which satisfies (4). The components of $\boldsymbol{v}$ in the spherical coordinates (r, θ, φ) are

$$\begin{pmatrix} v_r \\ v_\theta \\ v_\varphi \end{pmatrix} = \begin{pmatrix} \dfrac{L^2}{r} W \\ \dfrac{\partial}{\partial \theta}\left(\dfrac{\partial W}{\partial r} + \dfrac{W}{r} \right) \\ \dfrac{\partial}{\sin \theta\, \partial \varphi}\left(\dfrac{\partial W}{\partial r} + \dfrac{W}{r} \right) \end{pmatrix} \tag{7}$$

where L is the differential operator with respect to θ and φ:

$$L^2 = -\frac{1}{\sin \theta}\left\{ \frac{\partial}{\partial \theta}\left(\sin \theta \frac{\partial}{\partial \theta} \right) + \frac{1}{\sin \theta} \frac{\partial^2}{\partial \varphi^2} \right\}. \tag{8}$$

Taking the curl of (1), and taking (5) and (7) into consideration, the differential equation of W is obtained as

$$\nabla^4 W = -\frac{g_0}{\mu b} \rho. \tag{9}$$

Meanwhile, eliminating T from (2) and (3), and taking (6) and (7) into consideration, the differential equation of ρ is obtained as

$$\nabla^2 \rho = \frac{2\alpha\beta\rho_0}{k} L^2 W. \tag{10}$$

Then, substitution of (9) into (10) gives

$$\nabla^6 \rho = -\frac{2\alpha\beta g_0}{\nu k b} L^2 \rho, \tag{11}$$

where

$$\nu = \frac{\mu}{\rho_0} \tag{12}$$

is the kinematic coefficient of viscosity. The solution of (11) determines the density anomaly, and then the velocity field is evaluated by substituting the obtained value of ρ into (9).

3. Analytical Solutions

Suppose the density anomaly is expressed in a summation of spherical surface harmonic terms:

$$\rho = \sum_{n=2}^{\infty} \rho_n(r) Y_n(\theta, \varphi) \tag{13}$$

with an arbitrary radial function ρ_n of degree n. Here, it is assumed that the summation does not include both the zeroth and the first degree

terms. The physical meaning of this assumption is that the mean density anomaly of the asthenosphere is zero and its gravity center is located at the origin of the coordinates.

The spherical surface harmonic function Y_n has a relation

$$L^2 Y_n = n(n+1) Y_n \,, \tag{14}$$

so that (11) is rewritten as

$$(D^6 + \lambda^6) \rho_n = 0 \,, \tag{15}$$

where D is the differential operator with respect to r, which is defined by

$$D^2 = \frac{d^2}{dr^2} + \frac{2}{r} \frac{d}{dr} - \frac{n(n+1)}{r^2} \,. \tag{16}$$

In the expression of (15), λ is defined by

$$\lambda = \frac{1}{b} \{ R\ n(n+1) \}^{1/6} \,, \tag{17}$$

where

$$R = \frac{2\alpha\beta g_0 b^5}{k\nu} \tag{18}$$

corresponds to the Rayleigh number. The parameter λ having the dimension of a reciprocal length is used instead of R in this study.

The solution of (15) is easily obtained in the form:

$$\rho_n = C_1 h_n^{(1)}(\lambda r) + C_2 h_n^{(2)}(\lambda r) + C_3 h_n^{(1)}(\omega \lambda r)$$

$$+ C_4 h_n^{(2)}(\omega \lambda r) + C_5 h_n^{(1)}(\omega^2 \lambda r) + C_6 h_n^{(2)}(\omega^2 \lambda r) \tag{19}$$

using spherical Hankel functions of the first and the second kind with six coefficients to be determined by boundary conditions. ω and ω^2 are solutions of a cubic equation $x^3 - 1 = 0$, *i.e.*

$$\omega = \frac{-1 + \sqrt{3}\,i}{2} \,, \qquad \omega^2 = \frac{-1 - \sqrt{3}\,i}{2} \,. \tag{20}$$

Similarly to (13), W is expressed in a spherical surface harmonic series with the exception of the zeroth and first degree terms:

$$W = \sum_{n=2}^{\infty} W_n(r) Y_n(\theta, \varphi) \,, \tag{21}$$

together with

$$W_n = -\frac{g_0}{\mu b \lambda^4}\{C_1 h_n^{(1)}(\lambda r) + C_2 h_n^{(2)}(\lambda r) + \omega^2 C_3 h_n^{(1)}(\omega \lambda r)$$

$$+ \omega^2 C_4 h_n^{(2)}(\omega \lambda r) + \omega C_5 h_n^{(1)}(\omega^2 \lambda r) + \omega C_6 h_n^{(2)}(\omega^2 \lambda r)\} . \tag{22}$$

The velocity field is described by using W_n as

$$\begin{pmatrix} v_r \\ v_\theta \\ v_\varphi \end{pmatrix} = \sum_{n=2}^{\infty} \begin{pmatrix} \dfrac{n(n+1)}{r} W_n Y_n \\ \left(\dfrac{\mathrm{d}W_n}{\mathrm{d}r} + \dfrac{W_n}{r}\right)\dfrac{\partial Y_n}{\partial \theta} \\ \left(\dfrac{\mathrm{d}W_n}{\mathrm{d}r} + \dfrac{W_n}{r}\right)\dfrac{\partial Y_n}{\sin\theta\,\partial\varphi} \end{pmatrix} . \tag{23}$$

The density anomaly and the velocity field can be evaluated respectively by (19) and (23) after the six coefficients C_i $(i=1, 2, \cdots, 6)$ are determined by the boundary conditions.

4. Boundary Conditions

The upper mantle consists of a lithosphere about 100-km thick, underlaid by an asthenosphere having a thickness of 200 to 300-km. Based on the observational fact of S-wave attenuation and the existence of a low-velocity layer, the asthenosphere is considered to be partially melted, *i. e.*, "fluid" in a general sense. The bottom of the asthenosphere is not sharp, probably because of the gradual transition to the mesosphere due to partial mineralogical phase changes.

In our model, the temperature anomaly distribution in the lithosphere is characterized by the thermal conduction, and in the asthenosphere, is characterized by the thermal transportation due to convection flows.

The equation of thermal conduction

$$\nabla^2 T = 0 \tag{24}$$

governs the thermal state in the lithosphere, while the equations of thermal convection are satisfied in the underlying asthenosphere. The horizontal motion of the lithospheric plate can be neglected in our case because the crossterms of the horizontal velocity and the horizontal gradient of static temperature are considered to be small as compared with the conduction terms.

4.1 *Lithosphere*

If the solution of (24) is described in a form similar to (13) or (21):

$$T = \sum_{n=2}^{\infty} T_n(r) Y_n(\theta, \varphi) , \tag{25}$$

the radial function has the following form:

$$T_n(r) = A r^n + B r^{-n-1} , \tag{26}$$

where A and B are coefficients to be determined by the boundary conditions. The summation in (25) does not include the zeroth and first degree terms in accordance with the temperature anomaly in the asthenosphere.

The outer and the inner radii of the lithosphere are denoted by a and b, respectively. The boundary conditions of the lithosphere are that the temperature anomaly is zero and that the terrestrial heat flow anomaly is given on the earth's surface, *i. e.*, the outer surface of the lithosphere. Both values are continuous to those in the asthenosphere on the lower boundary surface.

The boundary conditions on the earth's surface are described as

$$\left.\begin{array}{l} T_n(a) = 0 , \\[2mm] \left[\dfrac{d T_n}{d r} \right]_{r=a} = - \dfrac{F_n(a)}{K_1} , \end{array}\right\} \tag{27}$$

where K_1 is the thermal conductivity of the lithospheric material and $F_n(a)$ is a determinable quantity from the heat flow data $F(\theta, \varphi)$ observed on the earth's surface, *i. e.*,

$$F(\theta, \varphi) = \sum_{n=2}^{\infty} F_n(a) Y_n(\theta, \varphi) . \tag{28}$$

Similarly to (25), the summation excludes the zeroth and first degree terms.

The boundary conditions (27) determine A and B, and then the radial temperature function becomes

$$T_n(r) = - \frac{a F_n(a)}{K_1(2n+1)} \left\{ \left(\frac{r}{a} \right)^n - \left(\frac{a}{r} \right)^{n+1} \right\} . \tag{29}$$

The heat flow in the radial direction on an arbitrary interface in the lithosphere is obtained from (29) as

$$F_n(r) = \frac{F_n(a)}{2n+1} \left\{ n \left(\frac{r}{a} \right)^{n-1} + (n+1) \left(\frac{a}{r} \right)^{n+2} \right\} . \tag{30}$$

$T_n(b)$ and $F_n(b)$ are continuous to the related values of the convection solutions on the lithosphere-asthenosphere boundary.

4.2 *Asthenosphere*

At the boundary between the lithosphere and the asthenosphere, the radial fluid velocity and the deviatoric shear stress are assumed to be zero, and the temperature anomaly and the heat flow anomaly are assumed to be continuous. On the other hand, the asthenosphere-mesosphere boundary conditions assume the radial and horizontal fluid velocities to be zero. These are described respectively as

$$
\left.\begin{aligned}
&W_n(b)=0 \\[2pt]
&\left[\frac{\mathrm{d}^2 W_n}{\mathrm{d}r^2}\right]_{r=b}=0 \\[2pt]
&\rho_n(b)=-\alpha\rho_0 T_n(b) \\[2pt]
&\left[\frac{\mathrm{d}\rho_n}{\mathrm{d}r}\right]_{r=b}=-\frac{\alpha\rho_0}{K}F_n(b) \\[2pt]
&W_n(c)=0 \\[2pt]
&\left[\frac{\mathrm{d}W_n}{\mathrm{d}r}\right]_{r=c}=0
\end{aligned}\right\}
\tag{31}
$$

where the inner radius of the asthenosphere is denoted by c, and K is the conductivity of the asthenosphere.

In the above, the shear stress condition is derived as follows. The shear stress with respect to r and θ is written by a spherical surface harmonic series:

$$
\tau_{r\theta}=\mu\left(\frac{\partial v_\theta}{\partial r}-\frac{v_\theta}{r}+\frac{1}{r}\frac{\partial v_r}{\partial\theta}\right)
$$

$$
=\mu\sum_{n=2}^{\infty}\left\{\frac{\mathrm{d}^2 W_n}{\mathrm{d}r^2}+\frac{(n-1)(n+2)}{r^2}W_n\right\}\frac{\partial Y_n}{\partial\theta}.
$$

It can be easily seen that the condition $\tau_{r\theta}=0$ at $r=b$ becomes $[\mathrm{d}^2 W_n/\mathrm{d}r^2]_{r=b}=0$ because of $W_n(b)=0$. The shear stress with respect to r and φ

$$
\tau_{r\varphi}=\mu\left(\frac{\partial v_\varphi}{\partial r}-\frac{v_\varphi}{r}+\frac{1}{r\sin\theta}\frac{\partial v_r}{\partial\varphi}\right)
$$

arrives at a similar condition.

For determining the six coefficients from the boundary conditions (31), we rewrite them as follows:

$$X + \omega^2 Y + \omega Z = 0$$

$$X + \omega Y + \omega^2 Z - \frac{2}{\lambda b}(X' + Y' + Z') = 0$$

$$X + Y + Z = \left(\frac{b}{a}\right)^n - \left(\frac{a}{b}\right)^{n+1}$$

$$n(X + Y + Z) - \lambda b(X' + \omega Y' + \omega^2 Z')$$

$$= \frac{K_1}{K}\left\{ n\left(\frac{b}{a}\right)^n + (n+1)\left(\frac{a}{b}\right)^{n+1}\right\}$$

$$P + \omega^2 Q + \omega R = 0$$

$$P' + Q' + R' = 0$$

(32)

where, for simplicity, we put

$$
\begin{pmatrix} X \\ Y \\ Z \\ X' \\ Y' \\ Z' \\ P \\ Q \\ R \\ P' \\ Q' \\ R' \end{pmatrix} = \frac{K_1(2n+1)}{\alpha \rho_0 a F_n(a)}
\begin{pmatrix}
C_1 h_n^{(1)}(\lambda b) + C_2 h_n^{(2)}(\lambda b) \\
C_3 h_n^{(1)}(\omega \lambda b) + C_4 h_n^{(2)}(\omega \lambda b) \\
C_5 h_n^{(1)}(\omega^2 \lambda b) + C_6 h_n^{(2)}(\omega^2 \lambda b) \\
C_1 h_{n+1}^{(1)}(\lambda b) + C_2 h_{n+1}^{(2)}(\lambda b) \\
C_3 h_{n+1}^{(1)}(\omega \lambda b) + C_4 h_{n+1}^{(2)}(\omega \lambda b) \\
C_5 h_{n+1}^{(1)}(\omega^2 \lambda b) + C_6 h_{n+1}^{(2)}(\omega^2 \lambda b) \\
C_1 h_n^{(1)}(\lambda c) + C_2 h_n^{(2)}(\lambda c) \\
C_3 h_n^{(1)}(\omega \lambda c) + C_4 h_n^{(2)}(\omega \lambda c) \\
C_5 h_n^{(1)}(\omega^2 \lambda c) + C_6 h_n^{(2)}(\omega^2 \lambda c) \\
C_1 h_{n+1}^{(1)}(\lambda c) + C_2 h_{n+1}^{(2)}(\lambda c) \\
C_3 h_{n+1}^{(1)}(\omega \lambda c) + C_4 h_{n+1}^{(2)}(\omega \lambda c) \\
C_5 h_{n+1}^{(1)}(\omega^2 \lambda c) + C_6 h_{n+1}^{(2)}(\omega^2 \lambda c)
\end{pmatrix}
$$

(33)

Eliminating the six coefficients from (33), we obtain

$$P = \frac{\lambda^2 b^2}{2i}(B_0 X - A_0 X')$$

$$Q = \frac{\omega^2 \lambda^2 b^2}{2i}(B_1 Y - A_1 Y')$$

$$R = \frac{\omega \lambda^2 b^2}{2i}(B_2 Z - A_2 Z')$$

$$P' = \frac{\lambda^2 b^2}{2i}(A_0'X - B_0'X') \left.\phantom{\frac{1}{2}}\right\} \quad \text{(34)}$$

$$Q' = \frac{\omega^2 \lambda^2 b^2}{2i}(A_1'Y - B_1'Y')$$

$$R' = \frac{\omega \lambda^2 b^2}{2i}(A_2'Z - B_2'Z')$$

where

$$
\begin{aligned}
A_0 &= H_{n,n}(\lambda b, \lambda c) \\
B_0 &= H_{n+1,n}(\lambda b, \lambda c) \\
A_0' &= H_{n+1,n+1}(\lambda b, \lambda c) \\
B_0' &= H_{n,n+1}(\lambda b, \lambda c) \\
A_1 &= H_{n,n}(\omega \lambda b, \omega \lambda c) \\
B_1 &= H_{n+1,n}(\omega \lambda b, \omega \lambda c) \\
A_1' &= H_{n+1,n+1}(\omega \lambda b, \omega \lambda c) \\
B_1' &= H_{n,n+1}(\omega \lambda b, \omega \lambda c) \\
A_2 &= H_{n,n}(\omega^2 \lambda b, \omega^2 \lambda c) \\
B_2 &= H_{n+1,n}(\omega^2 \lambda b, \omega^2 \lambda c) \\
A_2' &= H_{n+1,n+1}(\omega^2 \lambda b, \omega^2 \lambda c) \\
B_2' &= H_{n,n+1}(\omega^2 \lambda b, \omega^2 \lambda c)
\end{aligned}
\quad \text{(35)}
$$

by defining

$$H_{n,m}(z, z') = h_n^{(2)}(z)h_m^{(1)}(z') - h_n^{(1)}(z)h_m^{(2)}(z').$$

It can be shown that, for an arbitrary spherical Hankel function of degree n, the following relation holds

$$H_{n+1,n}(z, z) = \frac{2i}{z^2},$$

which is used for deriving (34).

Finally, the solutions of (32) are obtained as

$$X = \frac{D}{3} + \frac{2}{3\lambda b}(X' + Y' + Z')$$

$$Y = \frac{D}{3} + \frac{2\omega^2}{3\lambda b}(X' + Y' + Z')$$

$$Z = \frac{D}{3} + \frac{2\omega}{3\lambda b}(X' + Y' + Z')$$

$$X' = \frac{1}{\Delta}\left\{(M' - \omega^2 N')(\omega^2 I - NE) - (M - \omega^2 N)(\omega^2 I' - N'E)\right\}$$

$$Y' = \frac{1}{\Delta}\left\{(N' - \omega^2 L')(I - LE) - (N - \omega^2 L)(I' - L'E)\right\}$$

$$Z' = \frac{1}{\Delta}\left\{(M - \omega L)(I' - L'E) - (M' - \omega L')(I - LE)\right\}$$

(36)

where

$$D = \left(\frac{b}{a}\right)^n - \left(\frac{a}{b}\right)^{n+1}$$

$$E = \frac{nD}{\lambda b} - \frac{K_1}{K\lambda b}\left\{n\left(\frac{b}{a}\right)^n + (n+1)\left(\frac{a}{b}\right)^{n+1}\right\}$$

$$I = \frac{D}{3}(B_0 + \omega B_1 + \omega^2 B_2)$$

$$I' = \frac{D}{3}(A_0' + \omega^2 A_1' + \omega A_2')$$

$$L = A_0 - \frac{2}{3\lambda b}(B_0 + B_1 + B_2)$$

$$M = \omega A_1 - \frac{2}{3\lambda b}(B_0 + B_1 + B_2)$$

$$N = \omega^2 A_2 - \frac{2}{3\lambda b}(B_0 + B_1 + B_2)$$

$$L' = B_0' - \frac{2}{3\lambda b}(A_0' + \omega A_1' + \omega^2 A_2')$$

$$M' = \omega^2 B_1' - \frac{2}{3\lambda b}(A_0' + \omega A_1' + \omega^2 A_2')$$

$$N' = \omega B_2' - \frac{2}{3\lambda b}(A_0' + \omega A_1' + \omega^2 A_2')$$

$$\Delta = (M - \omega L)(N' - \omega^2 L') - (N - \omega^2 L)(M' - \omega L')$$

(37)

Substitutions of (37) into (36) give X, Y, Z, X', Y' and Z', and then P, Q, R, P', Q' and R' are determined by the relations (34). Instead of the six coefficients C_i $(i = 1, 2, \cdots, 6)$, these twelve quantities provide the

boundary values. The density anomaly and the velocity field in the asthenosphere are represented as

$$\rho_n = \frac{\alpha\rho_0\lambda^2 ab^2 F_n(a)}{2iK_1(2n+1)} \{XH_{n+1,n}(\lambda b,\ \lambda r) - X'H_{n,n}(\lambda b,\ \lambda r)$$

$$+ \omega^2 YH_{n+1,n}(\omega\lambda b,\ \omega\lambda r) - \omega^2 Y'H_{n,n}(\omega\lambda b,\ \omega\lambda r)$$

$$+ \omega ZH_{n+1,n}(\omega^2\lambda b,\ \omega^2\lambda r) - \omega Z'H_{n,n}(\omega^2\lambda b,\ \omega^2\lambda r)\} \qquad (38)$$

and

$$W_n = -\frac{\alpha\rho_0 ab g_0 F_n(a)}{2i\mu\lambda^2 K_1(2n+1)} \{XH_{n+1,n}(\lambda b,\ \lambda r) - X'H_{n,n}(\lambda b,\ \lambda r)$$

$$+ \omega YH_{n+1,n}(\omega\lambda b,\ \omega\lambda r) - \omega Y'H_{n,n}(\omega\lambda b,\ \omega\lambda r)$$

$$+ \omega^2 ZH_{n+1,n}(\omega^2\lambda b,\ \omega^2\lambda r) - \omega^2 Z'H_{n,n}(\omega^2\lambda b,\ \omega^2\lambda r)\} . \qquad (39)$$

It can be easily demonstrated that both (38) and (39) satisfy the boundary conditions (31).

By the way, the horizontal fluid velocity components are obtained from

$$\frac{dW_n}{dr} + \frac{W_n}{r} = \frac{n+1}{r}W_n + \frac{\alpha\rho_0 ab g_0 F_n(a)}{2i\mu\lambda K_1(2n+1)}$$

$$\cdot \{XH_{n+1,n+1}(\lambda b,\ \lambda r) - X'H_{n,n+1}(\lambda b,\ \lambda r)$$

$$+ \omega^2 YH_{n+1,n+1}(\omega\lambda b,\ \omega\lambda r) - \omega^2 Y'H_{n,n+1}(\omega\lambda b,\ \omega\lambda r)$$

$$+ \omega ZH_{n+1,n+1}(\omega^2\lambda b,\ \omega^2\lambda r) - \omega Z'H_{n,n+1}(\omega^2\lambda b,\ \omega^2\lambda r)\} . \qquad (40)$$

Especially on the upper boundary, it becomes

$$\left[\frac{dW_n}{dr} + \frac{W_n}{r}\right]_{r=b} = \frac{\alpha\rho_0 ag_0 F_n(a)}{\mu\lambda^3 b K_1(2n+1)}(X' + Y' + Z') .$$

This value is proved to be real.

5. Convection-Induced Gravity Field

The gravity disturbing potential outside the earth induced by convection currents is expressed as the integration of the density anomaly over the entire volume of the asthenosphere. That is

$$U = G\int_0^{2\pi} d\varphi' \int_0^{\pi} \sin\theta' d\theta' \int_c^b \frac{\rho(r',\ \theta',\ \varphi')}{l} r'^2 dr' \qquad (41)$$

where G is Newton's gravitational constant and l is the distance between the attracted point $(r,\ \theta,\ \varphi)$ and a mass element $(r',\ \theta',\ \varphi')$. The reciprocal

of l is given in a Legendre polynomial series

$$\frac{1}{l} = \frac{1}{r} \sum_{n=0}^{\infty} \left(\frac{r'}{r}\right)^n P_n(\cos \phi) \tag{42}$$

for $r > r'$, where ϕ, the angle between the attracted point and the mass element, is defined by the cosine law of a spherical triangle:

$$\cos \phi = \cos \theta \cos \theta' + \sin \theta \sin \theta' \cos (\varphi - \varphi') .$$

Substitutions of (13) and (42) into (41) give the potential field in the form of a spherical harmonic expansion:

$$U = \frac{4\pi G}{r} \sum_{n=2}^{\infty} \frac{Y_n}{2n+1} \int_c^b \rho_n(r')\left(\frac{r'}{r}\right)^n r'^2 \mathrm{d}r' . \tag{43}$$

The spherical Hankel function has the advantage that the integral in (43) can be analytically evaluated by using the solutions:

$$\int_c^b h_n^{(1)}(\lambda r') r'^{n+2} \mathrm{d}r' = \frac{1}{\lambda} \{b^{n+2} h_{n+1}^{(1)}(\lambda b) - c^{n+2} h_{n+1}^{(1)}(\lambda c)\} .$$

and a similar solution for $h_n^{(2)}(\lambda r')$. If the potential field is defined as

$$U = \sum_{n=2}^{\infty} \left(\frac{a}{r}\right)^{n+1} U_n(a) Y_n(\theta, \varphi) \tag{44}$$

for $r > a$, the weight function $U_n(a)$ has the form:

$$U_n(a) = \frac{4\pi G \alpha \rho_0 a^2 F_n(a)}{K_1 \lambda (2n+1)^2} \left\{ \left(\frac{b}{a}\right)^{n+2} (X' + \omega^2 Y' + \omega Z') \right.$$

$$\left. - \left(\frac{c}{a}\right)^{n+2} (P' + \omega^2 Q' + \omega R') \right\} . \tag{45}$$

$U_n(a)$ is proved to take a real value. Thus the convection-induced gravity potential outside the earth can be calculated from the known values of X', Y', Z', P', Q' and R'.

The related gravity anomaly is then calculated by differentiating the potential with respect to r and putting $r = a$, *i. e.*

$$\Delta g = -\left[\frac{\partial U}{\partial r}\right]_{r=a} = \sum_{n=2}^{\infty} \Delta g_n(a) Y_n(\theta, \varphi)$$

$$= \frac{1}{a} \sum_{n=2}^{\infty} (n+1) U_n(a) Y_n(\theta, \varphi) . \tag{46}$$

For verifying the existence of convection flows in the earth's asthenosphere, the gravity anomaly calculated for a postulated convection model

is compared with the actually observed gravity anomaly such as the gravity anomaly derived from the satellite orbit analyses. The gravity anomaly defined by (46), however, does not correspond to "gravity anomaly" defined in physical geodesy but to "gravity disturbance" (HEISKANEN and MORITZ, 1967). The satellite-derived gravity anomaly, which is reduced to the undulated surface of the geoid, includes a free-air gravity effect of the geoidal height. In the strict sense, the gravity anomaly calculated by (46) is preferably compared with the satellite-derived gravity disturbance but not with the satellite-derived gravity anomaly, although differences between these two geodetic quantities are practically insignificant.

6. Actual Calculations

6.1 *Heat Flow and Gravity Data*

The global heat flow data is presented by CHAPMAN and POLLACK (1975) in the form of spherical surface harmonic series with the fully-normalized Legendre function $P_{nm}(\cos \theta)$ up to $n=12$ degrees. The coefficients A_{nm} and B_{nm} of series expansion

$$F_n(a)Y_n(\theta, \varphi) = \sum_{m=0}^{n} (A_{nm} \cos m\varphi + B_{nm} \sin m\varphi)P_{nm}(\cos \theta) \qquad (47)$$

are used for our calculations. Fig. 1 shows the world heat flow chart obtained by summing up the series, except for the zeroth and first degree terms. Hence, Fig. 1 is somewhat different from CHAPMAN and POLLACK's original chart.

As can be seen in this chart, high heat flow zones (stippled areas in Fig. 1) coincide with the East-Pacific Rise, the Mid-Atlantic Ridge, the Mid-Indian Ocean Ridge, etc., which are known as convection sources by geophysical observations. The Far-East and Indonesian island-arcs form the western side of the circum-Pacific belt of high heat flow. The heat flow lows expected there along the ocean trenches are swallowed up by the relatively extensive heat flow highs predominantly occupying the marginal seas. The heat flow highs also match the tectonic features even up to the small details such as the Red Sea, the Hawaiian hot-spots, and the Caribbean island-arcs.

Fig. 2a shows the satellite-derived gravity disturbance corresponding to the 1973 Smithsonian Standard Earth III (GAPOSCHKIN, 1973). The stippled areas in this map indicate positive gravity disturbance with a contour interval of $0.2 \ \mathrm{mm \cdot s^{-2}}$. The original set consists of spherical sur-
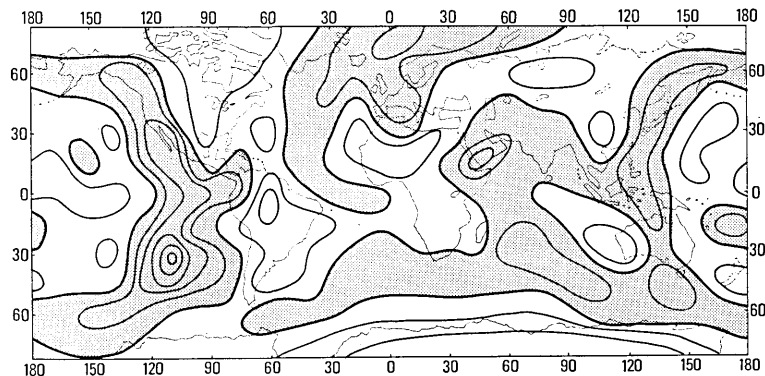
Fig. 1. Global heat flow (after CHAPMAN and POLLACK, 1975). Stippled areas represent high heat flow anomalies. Contour interval is 10 mW·m^{-2}.

face harmonic coefficients up to $n=36$ for zonal terms and $n=24$ for non-zonal terms, but in Fig. 2a the degree terms higher than $n=12$ are truncated for comparing with the gravity anomaly calculated from the Chapman and Pollack heat flow data.

As seen in this map, the amplitude of the gravity disturbance is about 0.5 mm·s^{-2} at maximum. If an isostatic balance should not exist in the crust-mantle system, the effect of topographic masses on the gravity field would amount to several mm·s^{-2}, *i. e.*, ten times larger than the amplitude of the real gravity disturbance field. In fact, the gravity disturbance is not correlated with the topographic effect on gravity of Fig. 2b, which is evaluated from the spherical surface harmonic coefficients of the earth's topographic elevation (LEE and KAULA, 1967). This implies that most of the topographic effect is isostatically compensated and the satellite orbit can not be largely affected by both the topographic irregularities and the undulation of the Mohorovicic discontinuity. Accordingly, the satellite-derived gravity disturbance is a deviation from the isostatic balance and can possibly represent the upper mantle structure.

The dominating high gravity disturbance in Fig. 2a are clearly located along the Far-East and Indonesian island-arcs and the Andes of South America. The geophysical implications of these gravity highs may be dense fluid materials of down-going convection currents around the ocean trenches. On the other hand, the low gravity disturbance zones coincide with the East-Pacific Rise and the Mid-Indian Ocean Ridge. Such coincidences can be explained by the distribution of low density materials over the convection sources.

In contrast to the East-Pacific Rise, the Mid-Atlantic Ridge obviously has a positive gravity disturbance. In the Mid-Atlantic regions, there
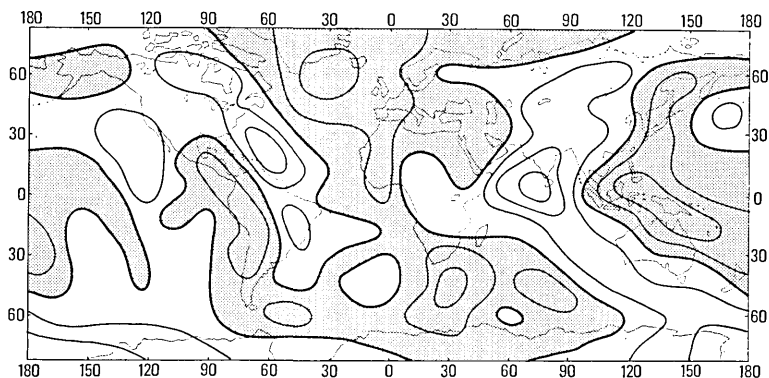
Fig. 2a. Satellite-derived gravity disturbance related to the 1973 Smith-sonian Standard Earth III (after GAPOSCHKIN, 1973). Stippled areas represent positive disturbances. Contour interval is $0.2\,\mathrm{mm \cdot s^{-2}}$ (20 mgal).
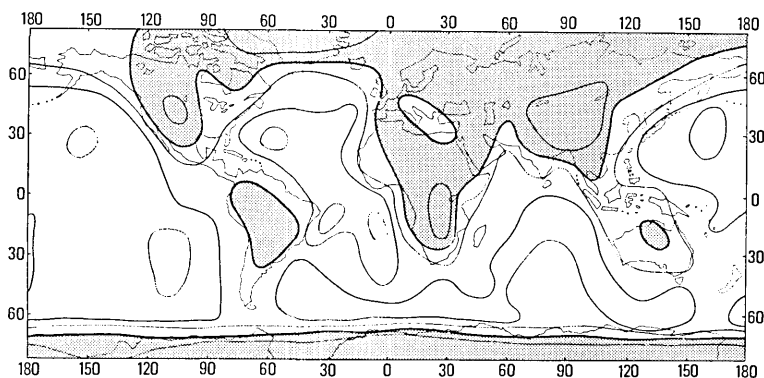

Fig. 2b. Topographic effect on the gravity field. Stippled areas represent positive anomalies. Contour interval is $2\,\mathrm{mm \cdot s^{-2}}$ (200 mgal).

exists nowhere negative contours which may result from an up-coming convection source. This is an unexpected result from a geophysical view-point in that the gravity disturbance should be negative over hot rising regions. An especially large positive disturbance around Iceland is ex-plained by KAULA (1969) that the gravitational attraction of extensive basaltic flows dominates convection-induced gravity disturbances. McKENZIE et al. (1974) proposed the case by numerical experiments that the gravity anomaly is positive over a hot rising region. Although many authors have discussed the comparison between the East-Pacific Rise and the Mid-Atlantic Ridge on the basis of topographical and geophysical obser-vations, the fundamental difference has not yet been completely clarified.

6.2 *Root Mean Square Anomalies*

The asthenosphere is presumed to be a spherical shell having a thickness of 200 to 300 km lying below a lithospheric shell having a thickness of about 100 km. In the model structure used in this study, the thickness of the lithosphere is fixed at 100 km throughout our calculations but that of the asthenosphere is taken as a variable ranging from 200 to 400 km. The other parameters chosen are $\alpha = 2 \times 10^{-5} \deg^{-1}$, $\beta = 2 \times 10^{-14} \deg \cdot cm^{-2}$, $\rho_0 = 3.5 \, g \cdot cm^{-3}$, $k = 2 \times 10^{-2} \, cm^2 \cdot s^{-1}$ and $K_1 = K = 2 \times 10^{-2} \, cal \cdot cm^{-1} \cdot s^{-1} \cdot deg^{-1}$ ($8.4 \, W \cdot m^{-1} \cdot deg^{-1}$). The coefficient of viscosity is uncertain but considered to play an important role in determining the convection behavior. Based on the vertical crustal motion due to the glacio-isostatic rebound, μ is chosen to be of an order of 10^{19} to $10^{21} \, N \cdot s \cdot m^{-2}$ for the present study.

Fig. 3a shows $\Delta g_n(a)/F_n(a)$, the weight function of convection-induced gravity anomaly per heat flow anomaly, against degrees of spherical surface harmonics for a 300-km thick asthenosphere model. Another weight function of horizontal fluid velocity on the upper boundary surface of the 300-km thick model, $[\mathrm{d}W_n/\mathrm{d}r]_{r=b}/F_n(a)$ is shown in Fig. 3b. As seen in these figures, the magnitudes of the weight functions become large for low degrees but rapidly converge to zero with an increasing n. This implies that both the calculated gravity anomaly and horizontal fluid velocity may be much affected by low-degree terms of heat flow anomaly.

In order to estimate the average size of the convection-induced gravity anomaly, the mean squares of Δg is considered:

$$\overline{\Delta g^2} = \frac{1}{4\pi} \int_0^{2\pi} \mathrm{d}\varphi \int_0^{\pi} \Delta g^2 \sin \theta \mathrm{d}\theta$$

$$= \sum_{n=2}^{\infty} \left\{ \frac{\Delta g_n(a)}{F_n(a)} \right\}^2 \sum_{m=0}^{n} (A_{nm}^2 + B_{nm}^2).$$

Four low-degree terms, *i. e.*, A_{20}, A_{21}, B_{21} and A_{40}, are omitted from the above summation for the purpose of a comparison with the satellite-derived gravity disturbance which does not include these four terms. The two terms, A_{21} and B_{21}, are proportional to the earth's products of inertia with respect to the y and x axes, respectively. They are essentially assumed to be zero because of the parallelism of the earth's rotation axis to the z axis. The other two terms, A_{20} and A_{40}, are defined as quantities determining the shape of an ellipsoid out of relation to the gravity disturbance field.

Similarly, the mean squares of horizontal fluid velocities on the upper boundary surface of the convection layer are estimated as
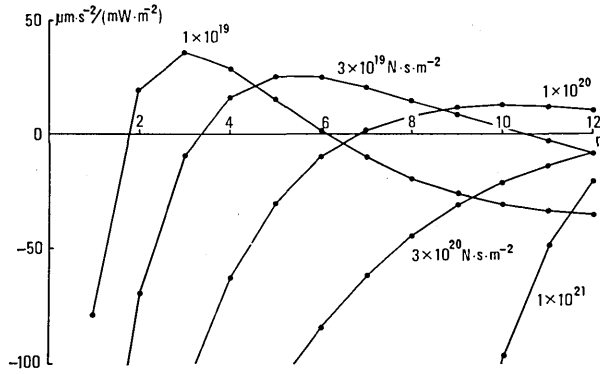
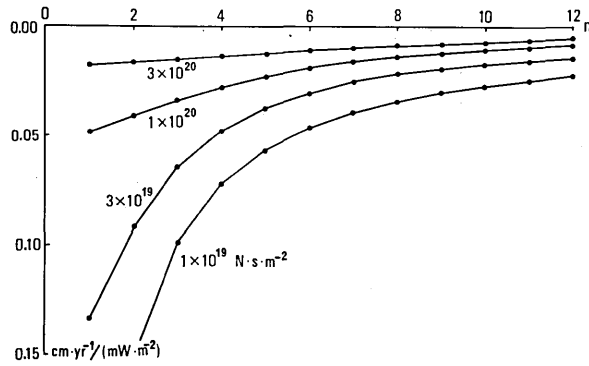Fig. 3a. $\Delta g_n(a)/F_n(a)$ in $\mu\text{m}\cdot\text{s}^{-2}/(\text{mW}\cdot\text{m}^{-2})$.

Fig. 3b. $[\text{d}W_n/\text{d}r]_{r=b}/F_n(a)$ in $\text{cm}\cdot\text{yr}^{-1}/(\text{mW}\cdot\text{m}^{-2})$.

$$\overline{[v_\theta^2+v_\varphi^2]}_{r=b} = \frac{1}{4\pi}\int_0^{2\pi}\text{d}\varphi\int_0^\pi [v_\theta^2+v_\varphi^2]_{r=b}\,\sin\theta\text{d}\theta$$

$$= \sum_{n=2}^\infty n(n+1)\left\{\frac{[\text{d}W_n/\text{d}r]_{r=b}}{F_n(a)}\right\}^2 \sum_{m=0}^n (A_{nm}^2+B_{nm}^2).$$

Furthermore, the mean squares of temperature anomaly on the lower boundary surface are also estimated as

$$\overline{T^2(c)} = \frac{1}{\alpha^2\rho_0^2}\sum_{n=2}^\infty \left\{\frac{\rho_n(c)}{F_n(a)}\right\}^2 \sum_{m=0}^n (A_{nm}^2+B_{nm}^2).$$

In these two cases, the summations include the above-mentioned four terms.

It can be shown that the variance of temperature anomaly on the upper boundary surface of the convection layer takes a constant value of about 140°C for our model. Substituting $r=b$ into (38), we obtain

$$T_n(b) = -\frac{\rho_n(b)}{\alpha\rho_0} = -\frac{aF_n(a)}{K_1(2n+1)}(X+Y+Z)$$

$$= - \frac{a F_n(a)}{K_1(2n+1)} \left\{ \left(\frac{b}{a} \right)^n - \left(\frac{a}{b} \right)^{n+1} \right\},$$

which is independent of the viscosity and the thickness of the convection layer. If the thickness of the lithosphere is denoted by δ_1, approximately we have

$$\left(\frac{b}{a} \right)^n - \left(\frac{a}{b} \right)^{n+1} \approx - \frac{\delta_1(2n+1)}{a},$$

because $\delta_1 \ll a$, so that

$$\frac{T_n(b)}{F_n(a)} \approx \frac{\delta_1}{K_1}.$$

As $\delta_1 = 100$ km and $K_1 = 2 \times 10^{-2}$ cal$\cdot$s$^{-1}\cdot$deg^{-1}(8.4 W$\cdot$m$^{-1}\cdot$deg^{-1}) are chosen and A_{nm} and B_{nm} given by CHAPMAN and POLLACK (1975) are used for our model, this weight function can be evaluated to be independently constant of n as follows:

$$\frac{T_n(b)}{F_n(a)} \doteq \frac{100}{8.4} \doteq 12 \ \text{deg/(mW} \cdot \text{m}^{-2}).$$

The root mean square anomaly is a very useful measure of the average size of gravity anomaly. Fig. 4a represents $\sqrt{\overline{\Delta g^2}}$ against the viscosity with parameters of the thickness of the asthenosphere. As can be seen in Fig. 2a, the satellite-derived gravity disturbance has the amplitude of 0.1 to 0.5 mm$\cdot$s^{-2}. Judging from this fact, a plausible convection model is 300-km thick with a viscosity less than 5×10^{19} N$\cdot$s$\cdot$m^{-2} (5×10^{20} poise) or 400-km thick with a viscosity less than 2×10^{20} N$\cdot$s$\cdot$m^{-2} (2×10^{21} poise). These orders of viscosity are consistent with those estimated from the glacio-isostatic vertical movement of the crust.

The horizontal fluid velocity on the upper boundary surface of the asthenosphere may be of the same order as that of the ocean-floor spreading, which is estimated to be a few cm/year according to the observed geomagnetic lineations. On the other hand, Fig. 4b shows the root mean squares of the calculated horizontal fluid velocity. This figure may suggest that a 200 to 400-km thick asthenosphere model with a viscosity less than 10^{20} N$\cdot$s$\cdot$m^{-2} would indicate a fluid velocity comparable with that of the ocean-floor spreading.

The root mean squares of temperature anomaly on the lower boundary surface of the convection layer are shown in Fig. 4c. Temperature anomalies of several hundred degrees centigrade can be realized in a lower part of the earth's real asthenosphere.
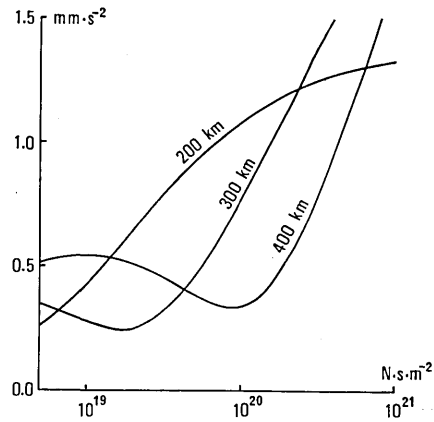
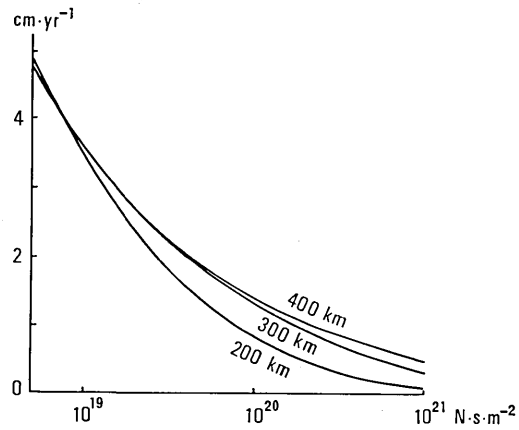Fig. 4a.   Root mean square gravity anomaly.

Fig. 4b.   Root mean square of horizontal fluid velocity
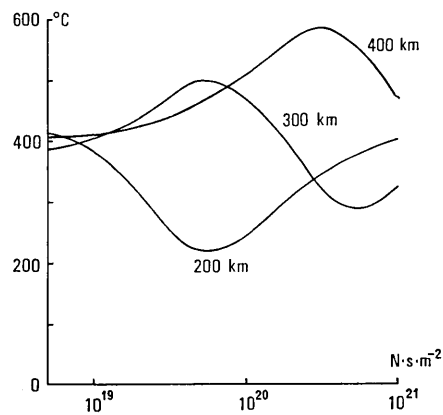on the lithosphere-asthenosphere boundary surface.

Fig. 4c.   Root mean square temperature anomaly on
the asthenosphere-mesosphere boundary surface.

6.3 *Best-fitting Convection Model*

The question whether or not the gravity anomaly calculated from the heat flow data matches the gravity disturbance derived from satellite orbit analyses is of great importance for examining the postulated convection hypothesis. A convection model may be valid only when the calculated gravity anomaly is consistent with the satellite-derived gravity disturbance. The best-fitting model should be selected so as to maximize the correlation coefficient between the calculated gravity anomaly and the satellite-derived gravity disturbance.

As previously described, the gravity anomaly calculated from the heat flow data is expressed as

$$\Delta g = \sum_{n=2}^{N} \frac{\Delta g_n(a)}{F_n(a)} \sum_{m=0}^{n} (A_{nm} \cos m\varphi + B_{nm} \sin m\varphi) P_{nm}(\cos \theta)$$

by using the spherical surface harmonic coefficients A_{nm} and B_{nm} of degree n less than N.

Meanwhile, the satellite-derived gravity disturbance has the form:

$$\delta g = g_0 \sum_{n=2}^{N} (n+1) \sum_{m=0}^{n} (C_{nm} \cos m\varphi + S_{nm} \sin m\varphi) P_{nm}(\cos \theta),$$

where g_0 is the mean gravity value observed on the earth's surface (HEISKANEN and MORITZ, 1967). Then the correlation coefficient between Δg and δg is

$$\frac{\displaystyle\sum_{n=2}^{N} \frac{(n+1)\Delta g_n(a)}{F_n(a)} \sum_{m=0}^{n} (A_{nm}C_{nm} + B_{nm}S_{nm})}{\sqrt{\displaystyle\sum_{n=2}^{N} \left\{\frac{\Delta g_n(a)}{F_n(a)}\right\}^2 \sum_{m=0}^{n} (A_{nm}^2 + B_{nm}^2) \cdot \sum_{n=2}^{N} (n+1)^2 \sum_{m=0}^{n} (C_{nm}^2 + S_{nm}^2)}}.$$

If Δg and δg are positively correlated, both the heat flow and the gravity anomaly are possibly related to a common generating source. If they are not correlated, the presupposed convection model may be inappropriate for a system connecting both the geophysical observation data.

Fig. 5 shows changes in the thus-obtained correlation coefficient with viscosity of asthenospheric materials. For example, in the case of a 300-km thick convection layer, the correlation coefficient has a maximum for a viscosity of 3.5×10^{19} N·s·m^{-2}. If the thickness of the asthenosphere is assumed to be 300 km, the related viscosity is lower by an order of magnitude than those obtained from the uplift of Fennoscandia and Lake Bonneville. As a matter of fact, the viscosity is not accurately determined by geophysical observations and could be in error by an order of

magnitude.

It is interesting to see in Fig. 5 that the curve for a thickness of 400-km has a form quite similar to that for a thickness of 300-km, but the maximum correlation point shifts from 3.5×10^{19} N·s·m^{-2} to 1.5×10^{20} N·s·m^{-2} with a ratio of $(4/3)^5$. This fact can be explained by the same Rayleigh number.
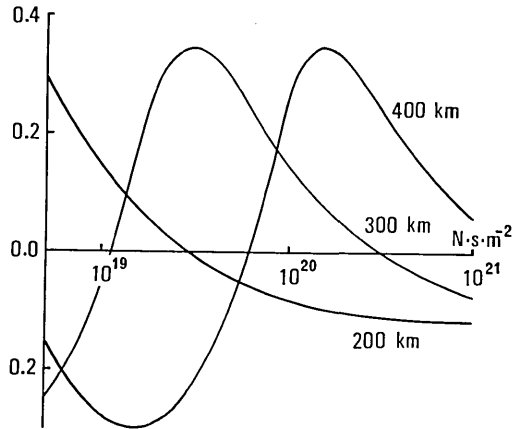
Fig. 5. Changes in correlation coefficient between the observed gravity anomaly and one calculated from global heat flow data.

6.4 *Calculated Gravity Anomaly and Related Convection*

The gravity anomaly calculated from the heat flow data assuming convection flows with a viscosity of 2×10^{19} N·s·m^{-2} is shown in Fig. 6a. For a comparison with the satellite-derived gravity disturbance, A_{20}, A_{21}, B_{21} and A_{40} are not taken into account in the calculations. It is clear that there exists an identical correlation between the major features of this map and those of the satellite-derived gravity map. It will be demonstrated that the calculated gravity anomalies match the observed ones, even up to some small details.

A first point to be noticed in our results is the fact that in Fig. 6a a positive anomaly zone occupies the Mid-Atlantic region. From a theoretical standpoint, a negative gravity anomaly is expected over a high heat flow region due to the thermal expansion of convecting materials. Nevertheless, as seen in Fig. 2a, the positive contours actually cover the high heat flow region in the northern part of the Atlantic Ocean. It should be reconsidered that this contradiction has not yet been explained properly, except for the numerical experimental results reported by McKENZIE *et al.* (1974). However, the contradiction is now solved by our

calculations, which result in a positive anomaly zone well consistent with that observed in the Mid-Atlantic regions. A similar consistency can also be pointed out for the negative zone located in the midst of the Asian continent and the Indian Ocean. Furthermore, the highly positive anomalies along the Far-East and Indonesian island-arcs satisfactorily match each other in both Figs. 2a and 6a. The completeness of the calculated gravity anomaly is evidenced by a good coincidence with detailed features of the observed gravity disturbance; for example, a highly positive anomaly centering in Iceland, an isolated positive one covering the Arabian peninsula, and a negative one widely located in the midst of the African continent.

On the other hand, in the East-Pacific Rise and its adjacent regions, the gravity anomalies in Fig. 6a seem to be rather inversely correlated with those in Fig. 2a. This may evidence that the physical properties of the asthenospheric materials under the East Pacific regions are different from those used throughout our calculations. One of the possibilities of this local difference is a thermal change in viscosity due to the comparatively high temperature under this region. The convection model calculation with a temperature-dependent viscosity, however, is beyond the scope of our present study.

Fig. 6b shows the temperature anomaly on the lithosphere-asthenosphere boundary surface. The pattern of this map closely resembles that of the heat flow map (Fig. 1). The maximum temperature anomaly is as high as 600°C at the heat flow crest in the East-Pacific Rise. The horizontal flows on the boundary surface are illustrated in Fig. 6c, where an arrow indicates the direction of fluid velocity and the length of the arrow is proportional to its magnitude. Sources and sinks of the convection current can be recognized as divergent and convergent flow vectors, respectively. Flow speed amounting to 6 cm/year or higher is comparable with the flow speed estimated from geophysical observation results. This implies that the convection model structure and the physical properties postulated in this paper are plausible.

According to the current theory of plate tectonics, the plate subduction along the Far-East deep-sea trenches is supposed to be driven by the westward convection currents spreading away from the East-Pacific Rise. Our calculation results, however, indicate oppositely directed convection currents along these trenches, as shown in Fig. 6c. This incompatibility is dependent on lack of heat flow lows along the trenches in the Chapman and Pollack global chart, in which the related lows are swallowed up by the highs which predominantly occupy the marginal
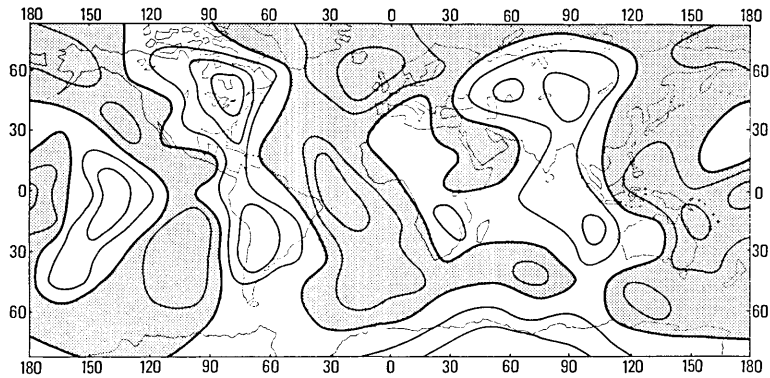
Fig. 6a. Gravity anomaly calculated from global heat flow data. Stippled areas represent positive anomalies. Contour interval is $0.2\,\mathrm{mm\cdot s^{-2}}$ (20 mgal).
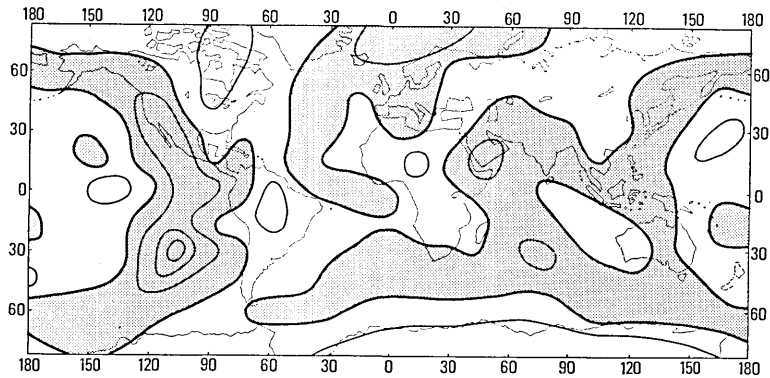

Fig. 6b. Temperature anomaly on the lithosphere-asthenosphere boundary surface. Stippled areas represent positive anomalies. Contour interval is 200°C.
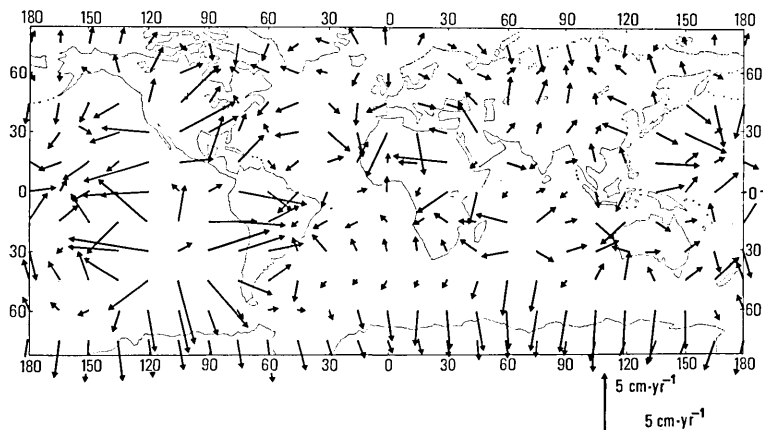

Fig. 6c. Horizontal currents on the lithosphere-asthenosphere boundary surface.

seas. Generally, the small-scaled anomalies can be neglected in the spherical surface harmonic representation of degrees as small as 12. With a higher-degree heat flow chart sufficiently expressing such a small-scaled heat flow anomaly, our calculation method can produce results comparable with the local problem of plate tectonics.

In order to see the vertical structure of convection, the temperature anomaly (Fig. 7a) and the currents (Fig. 7b) are illustrated in sections through the equator. If viewed from the earth's surface, each temperature anomaly, high or low, can be considered as a convection source or sink, respectively. Thermally driven convection currents go up to the source at the upper boundary of the layer, move horizontally away from the source to an adjacent sink, and then return downward.

As can be seen in these sections, the high temperature anomaly under the East-Pacific Rise seems to continue downwards to the bottom of the convection layer and the related convection currents rise from the bottom to the top. A megacell of convection stirs the fluid throughout the total depth of the asthenosphere. In contrast to the East-Pacific Rise,
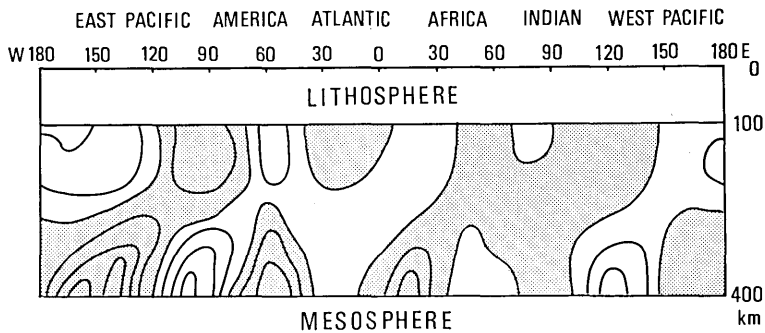
Fig. 7a. Vertical distribution of temperature anomaly on the equatorial section. Stippled areas represent positive anomalies. Contour interval is 200°C.
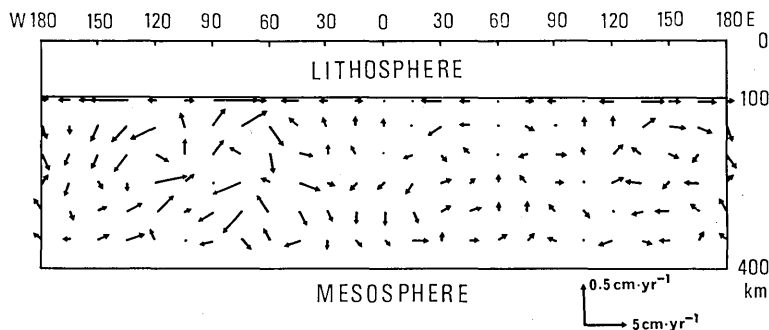
Fig. 7b. Fluid velocity on the equatorial section.

the Mid-Atlantic anomaly has no root with a pair of minor convection cells rolling near the surface. The wide distribution of low temperature and high density anomalies surrounding the Mid-Atlantic anomaly causes a positive gravity anomaly there. The effect of the near-surface Mid-Atlantic density low on gravity is overshadowed by the widely surrounding density highs. This is our explanation of the facts observed on the Mid-Atlantic Ridge, which seems contrary to the general belief that the gravity anomaly should be negative over the hot rising regions.

7. Conclusion

The preceding sections have concentrated on the analytical derivation of steady-state solutions of thermal convection currents in the earth's asthenosphere from the world heat flow data provided by CHAPMAN and POLLACK (1975). In order to test how the calculated gravity anomaly matches the gravity field obtained from the satellite orbit analyses and combined with the surface gravimetric results (GAPOSCHKIN, 1973), the correlation between both the gravity anomalies has been considered. If well correlated, the presupposed theoretical simplifications and physical properties of the convection model are justifiable. In fact, both gravity anomalies fit each other even in some models. For example, in Fig. 6a, the gravity anomaly calculated with a uniform viscosity of 2×10^{19} N·s·m^{-2} in a 300-km thick asthenosphere model is closely consistent with the satellite-derived gravity data, even to some small details (Fig. 2a).

Contrary to the positive gravity anomaly distributed over the Mid-Atlantic Ridge, there has existed the argument that the gravity anomaly should be negative over such hot rising regions because their density is relatively low. Nevertheless, the geophysical investigations have never properly explained this contradiction with the exception of McKenzie *et al.'s* idea of the contribution from the deformed surface. However, without any consideration of the surface relief, the present model calculations have completely solved the contradiction by the dominant contribution from the deeper structure. Furthermore, some consistencies between the observed and calculated gravity anomalies in the Mid-Asian continent, the Indian Ocean, the Far-East and Indonesian island-arcs, etc., are noted. Although our calculations are restricted to the simple convection models of a uniformly viscous fluid with some theoretical simplifications, such consistencies possibly confirm the completeness of the theoretical approach method and models used in this paper, and moreover evidence the existence of thermally driven convection currents in the earth's asthenosphere.

Acknowledgment

References

CHANDRASEKHAR, S., *Hydrodynamic and Hydromagnetic Stability*, Oxford Clarendon Press, Oxford, 1961.

CHAPMAN, D.S. and H.N. POLLACK, Global heat flow: A new look, *Earth Planet. Sc. Lett.*, 28, 23-32, 1975.

GAPOSCHKIN, E.M., 1973 Smithsonian Standard Earth III, Smithsonian Astrophys. Obs. Spec. Rep. 353, 1973.

HADDON, R.A.W. and K.E. BULLEN, An earth model incorporating free earth oscillation data, *Phys. Earth Planet. Inter.*, 2, 35-49, 1969.

HAGIWARA, Y., Linear transformation of gravity field and terrestrial heat flow assuming steady-state thermal convection currents, *Bull. Earthq. Res. Inst.*, 55, 369-385, 1980.

HEISKANEN, W. and H. MORITZ, *Physical Geodesy*, Freeman, San Francisco, 1967.

KAULA, W.M., A tectonic classification of the main features of the earth's gravitational field, *J. Geophys. Res.*, 74, 4807-4826, 1969.

KONO, Y., TSUZUKI, T. and A. YAMAMOTO, Simulation of the time-dependent thermal convection within the earth's mantle., *J. Phys. Earth*, 27, 315-336, 1979.

LEE, W.H.K. and W.M. KAULA, A spherical harmonic analysis of the earth's topography, *J. Geophys. Res.*, 72, 753-758, 1967.

McKENZIE, D.P., ROBERTS, J.M. and N.O. WEISS, Convection in the earth's mantle: towards a numerical simulation, *J. Fluid Mech.*, 62, 465-538, 1974.

RIKITAKE, T., Electrical conductivity and temperature in the earth, *Bull. Earthq. Res. Inst.*, 30, 13-24, 1952.

RUNCORN, S.K., Satellite gravity measurements and a laminar viscous flow model of the earth's mantle, *J. Geophys. Res.*, 69, 4389-4394, 1964.

28. 重力と熱流量データから推定した定常アセノスフェア対流

地震研究所　　萩　原　幸　男

　アセノスフェアに熱対流が存在するものと仮定して，グローバルな熱流量分布データから重力場を計算して，これが人工衛星重力とマッチするように，アセノスフェアの深さや粘性を決めようというのが本論文の目的である.

　まづ球殻を2分し，上部のリソスフェアは熱伝導のみ，下部のアセノスフェアにおいては熱対流によって熱が運ばれるものとし，摂動方程式の解を導く. 本来6個の境界条件によって解くのであるが，そのうち，アセノスフェア底面の温度条件のかわりに，リソスフェア表面に観測された熱流量分布を与える. つまり表面で温度勾配を与えることになる. 得られた解からブシネスク近似によって密度異常におきかえ，重力を求める.

　熱流量分布から計算した重力場を人工衛星重力乱れと比較してみると，例えば，厚さ 100 km のリソスフェアの下に，厚さ 300 km のアセノスフェアがあったとして，粘性 3.5×10^{19} N·s·m^{-2} のときに，両者はよい相関を示すことがわかった. 細部にわたっても，両者はかなりよい相関を示し，例えば中央大西洋海嶺では，アセノスフェア上部にある小さなローラーセルによって熱流量が高く，かつローラーセルの下部を広く占める冷えたセルの影響によって，正の重力異常が生じることがわかった. これに対して，東太平洋海膨の対流はアセノスフェア底部に達するほどの大きいメガセルをつくっていると考えられる.

　以上のように，熱流量分布から計算した重力場が，まったく独立に人工衛星軌道から得られた重力場にかなりよく一致するという事実は，採用したモデルの正しさもさることながら，アセノスフェアにおける熱対流機構の存在の可能性を示唆するものではなかろうか.